Impacts of Meteorological Uncertainties on the Haze Formation in Beijing-Tianjin-Hebei (BTH) during Wintertime: A case study

Naifang Bei[1], Jiarui Wu[2], Miriam Elser[3], Tian Feng[2], Junji Cao[2], Imad El-Haddad[3], Xia Li[2], Rujin Huang[2], Zhengqiang Li[4], Xin Long[2], Li Xing[2], Shuyu Zhao[2], Xuexi Tie[2], André S. H. Prévôt[3], and Guohui Li[2*]

[1]School of Human Settlements and Civil Engineering, Xi'an Jiaotong University, Xi'an, Shaanxi, China
[2]Key Lab of Aerosol Chemistry and Physics, SKLLQG, Institute of Earth Environment, Chinese Academy of Sciences, Xi'an, China
[3]Laboratory of Atmospheric Chemistry, Paul Scherrer Institute, 5232 Villigen, Switzerland
[4]State Environmental Protection Key Laboratory of Satellite Remote Sensing, Institute of Remote Sensing and Digital Earth, Chinese Academy of Sciences, Beijing, China

[*]Correspondence to: Guohui Li (ligh@ieecas.cn)

Abstract: In the present study, a persistent heavy haze episode from 13 to 20 January 2014 in Beijing-Tianjin-Hebei (BTH) is simulated using the WRF-CHEM model through ensemble simulations to investigate impacts of meteorological uncertainties on the haze formation. Model results show that uncertainties in meteorological conditions substantially influence the aerosol constituent simulations at an observation site in Beijing, and the ratio of the ensemble spread to ensemble mean (RESM) exceeds 50%. The ensemble mean generally preforms well in reproducing the fine particles ($PM_{2.5}$) temporal variations and spatial distributions against measurements in BTH. The meteorological uncertainties do not alter the $PM_{2.5}$ distribution pattern in BTH principally or dominate the haze formation and development, but remarkably affect the simulated $PM_{2.5}$ level, and the RESM for the simulated $PM_{2.5}$ concentrations can be up to 30% at the regional scale. In addition, the rather large RESM in $PM_{2.5}$ simulations at the city scale also causes difficulties in evaluation of the control strategies. Therefore, our results suggest that the ensemble simulation is imperative to take into account the impact of the meteorological uncertainties on the haze prediction.

1 Introduction

Over the past three decades, rapid industrialization and urbanization have caused severe air pollution in China, particularly during wintertime heavy haze with extremely high levels of fine particles ($PM_{2.5}$) frequently engulfs the north of China (e.g., Chan and Yao, 2008; Fang et al., 2009; Zhao et al., 2013; Huang et al., 2014; Guo et al., 2014; Wu et al., 2017; Li et al., 2017). Elevated atmospheric aerosols or $PM_{2.5}$ not only influence the Earth climate system, but also remarkably impair visibility and potentially cause severe health defects (e.g., Penner et al., 2001; Pope and Dockery, 2006; Zhang et al., 2007).

Meteorological condition is critical for understanding the formation, transformation, diffusion, transport, and removal of the pollutants in the atmosphere. Dabberdt et al. (2004) have listed the meteorological research needs for improving air quality forecasting, one of which is to provide the model uncertainty information through ensemble prediction capabilities and quantify uncertainties and feed-backs between meteorological and air quality modeling components. Numerous studies have been performed in China to explore the role of meteorological conditions in the air pollution formation (e.g., Gao et al., 2011; Zhang et al., 2012; Wu et al. 2013; Wang et al. 2014; Zhang et al. 2015; Bei et al. 2016a, b). Most recently, Liu et al. (2017) have investigated the meteorological impacts on the $PM_{2.5}$ concentrations over Beijing-Tianjin-Hebei (BTH) in December 2015. Their results have demonstrated that the unfavorable meteorological conditions are the main reason for deterioration of the air quality in BTH, while the undertaken emission control measures have only mitigated the air pollution slightly.

Previous studies on the air quality forecasting sensitivity to meteorological uncertainties mainly include Monte Carlo simulations (e.g. Dabberdt and Miller, 2000; Beekmann and Derognat, 2003) and adjoint sensitivity studies (e.g. Menut, 2003). The ensemble approach has also been applied to photochemical and secondary organic aerosol

(SOA) simulations in various numerical models (e. g. Galmarini et al., 2004; McKeen et al., 2005), photo-chemical reactions (e. g. Delle Monache and Stull, 2003), emission scenarios (e. g. Delle Monache et al., 2006), physical parameterizations (e. g. Mallet and Sportisse, 2006), and meteorological initial conditions (e. g. Zhang et al. 2007; Bei et al. 2012). The ensemble means have generally performed better than most of individual models. Uncertainties in meteorological initial conditions have been shown to substantially influence both ozone (O_3) and SOA simulations, including the peak time concentrations, the horizontal distributions, and the temporal variations (Zhang et al. 2007; Bei et al. 2012). Recently, Sharma et al. (2016) have evaluated uncertainties in surface O_3 simulations over the South Asian region during the pre-monsoon season due to different emission inventories and different chemical mechanisms. They have suggested that the assessment of the tropospheric O_3 budget and its implications on public health and agricultural output should be conducted prudently considering the huge uncertainties caused by emission inventories and chemical mechanisms. Solazzo et al. (2017) have emphasized the high interdependencies among meteorological and chemical variables and the related errors, indicating that the evaluation of the air quality model performance needs to be confirmed by more complementary analysis of meteorological fields and chemical precursors.

The purpose of the present study is to explore impacts of the uncertainties in meteorological conditions on the $PM_{2.5}$ simulations or forecasts in BTH through ensemble simulations using the WRF-CHEM model. The methodology and model are presented in Section 2. The analyses, results, and discussions are included in Section 3. The summary and conclusions are given in Section 4.

2 Model and Methodology

2.1 WRF-CHEM Model

A specific version of the WRF-CHEM model is used to examine impacts of the uncertainties in meteorological conditions on the $PM_{2.5}$ simulations or the haze formation in BTH, which is developed by Li et al. (2010; 2011a, b; 2012) at the Molina Center for Energy and the Environment. The model includes a new flexible gas phase chemical module and the CMAQ/Models-3 aerosol module developed by US EPA (Binkowski and Roselle, 2003). The inorganic aerosols are predicted using the ISORROPIA Version 1.7 (Nenes et al., 1998). The SOA formation is simulated using a non-traditional SOA module, including the volatility basis-set (VBS) modeling method and the SOA contributions from glyoxal and methylglyoxal. Detailed description of the WRF-CHEM model can be found in Li et al. (2010; 2011a, b; 2012). A persistent heavy haze pollution episode from 13 to 20 January 2014 in BTH is simulated. The model simulation domain is shown in Figure 1, and detailed model configurations can be found in Table 1.

2.2 Ensemble Initialization Method

The ensemble initialization method used in the present study is called "climatological ensemble initialization method" (Zhang et al., 2007; Bei et al., 2012). In the approach, dynamically consistent initial and boundary conditions are statistically sampled from a seasonal meteorological data set. In order to represent the wintertime climatological statistics, a data set during the period from 1 November 2013 to 28 February 2014 is generated using NCEP-FNL 1°×1° reanalysis data. The perturbed variables include the horizontal wind components, potential temperature, perturbation pressure, and mixing ratio of water vapor. Other prognostic variables such as vertical velocity and mixing ratios of hydrometeors are not perturbed. In general, the perturbation in horizontal wind components constitutes the most important uncertainty in those variables (Bei et al., 2008; 2010). Thirty ensemble members are randomly chosen from this climatological data set. Similarly, boundary conditions for each ensemble member are generated from the same data set beginning at the randomly

selected initial time of the given member, and extended for the same length of time as the simulated episode. Deviations of the initial and boundary condition data for each member from the climatological mean for the entire period are then scaled down to be 20% to reduce the ensemble spread to be less than typical observation error magnitudes (Nielsen-Gammon et al., 2007) and added to the unperturbed initial and boundary conditions derived directly from the NCEP-FNL analyses valid at 12:00 UTC on 12 January 2014, which are used for the 6-km domain ensemble simulation. Figures 2a–d show the vertical distribution of the average initial ensemble spread which is calculated as the standard deviation of the perturbations imposed on each ensemble member's initial field. The average spread is 0.5–3.0 m s^{-1} for horizontal winds (U and V component), 0.5–1.1 K for temperature, 0.02–0.48 hPa for pressure, and 0–0.15 g kg^{-1} for the water vapor mass mixing ratio. The initial ensemble spreads of meteorological variables are generally less than their typical observation error magnitudes. It is worth noting that all the ensemble simulations used the same initial and boundary conditions for chemical fields, as well as the same anthropogenic emission inventory.

2.3 Pollutants Measurements

The hourly near-surface CO, SO_2, NO_2, O_3, and $PM_{2.5}$ mass concentrations in BTH are released by the China's Ministry of Environmental Protection (China MEP) and can be downloaded from the website http://www.aqistudy.cn/. The Aerodyne High Resolution Time-of-Flight Aerosol Mass Spectrometer (HR-ToF-AMS) with a novel $PM_{2.5}$ lens is used to measure the sulfate, nitrate, ammonium, and organic aerosols (OA) from 9 to 26 January 2014 at the Institute of Remote Sensing and Digital Earth (IRSDE), Chinese Academy of Sciences (40.00°N, 116.38°E) in Beijing (Figure 1) (Williams et al., 2013). The Positive Matrix Factorization (PMF) technique is utilized with constraints implemented in SoFi (Canonaco et al., 2013) to analyze the sources of OA and five components are separated by

their mass spectra and time series. The components include hydrocarbon-like OA (HOA), cooking OA (COA), biomass burning OA (BBOA), coal combustion OA (CCOA), and oxygenated OA (OOA). HOA, COA, BBOA, and CCOA are interpreted for surrogates of primary OA (POA), and OOA is a surrogate for SOA. Detailed information about the HR-ToF-AMS measurements and data analysis can be found in Elser et al. (2016). A Lidar has also been deployed at IRSDE and the aerosol backscatter signal is used to retrieve the planetary boundary layer (PBL) height.

3 Results and Discussions

3.1 Synoptic Overview

Figure 3 shows temporal evolutions of the observed $PM_{2.5}$ mass concentrations averaged over 13 cities (see Figure 1) in BTH during the severe haze episode from 13 to 21 January 2014. The observed $PM_{2.5}$ mass concentrations are frequently higher than 250 μg m^{-3} in the 13 cities during the episode, exceeding the standard of severe pollutions (hourly $PM_{2.5}$ mass concentration exceeding 250 μg m^{-3}, Feng et al., 2016). The haze in BTH was in the stage of development from January 13 to 15, with the gradual increase of the $PM_{2.5}$ concentration. BTH was most polluted when the haze was in the maturity stage on January 16, with the $PM_{2.5}$ concentration exceeding 400 μg m^{-3} in most of the cities. From January 17 to 19, the $PM_{2.5}$ concentrations fluctuated considerably, which was primarily caused by the transition between different synoptic situations. During nighttime on January 19, the haze in BTH rapidly dissipated, with the $PM_{2.5}$ concentration decrease of several hundreds of μg m^{-3} in two or three hours. In addition, the diurnal cycles of the observed $PM_{2.5}$ mass concentrations were not clear, demonstrating the obvious regional pollution characteristics in BTH. For the four mega-cities in BTH, the $PM_{2.5}$ levels in Shijiazhuang and Baoding were

much higher than Beijing and Tianjin, which is caused by the massive local emissions in Shijiazhuang and Baoding.

NCEP-FNL reanalysis data is used to examine the effect of synoptic conditions on the air pollution during the haze episode in BTH. Figures s1-s3 show the synoptic conditions at the surface level, 850 hPa, and 500 hPa, respectively. On January 13, BTH is on the north of a high pressure at the surface level, causing the southerly wind in/on the east of BTH, and sandwiched between the trough in the northeast of BTH and the high pressure in the southwest of BTH at 850 hPa, inducing the westerly surface wind in the west of BTH. At 500 hPa, the BTH is situated in the rear of the trough, and the westerly airflow is dominant. The air pollutants in BTH are subject to be transported to the east but hindered by the southerly wind, causing accumulation of air pollutants. On January 14, the high pressure system begins to control BTH at the surface level and 850 hPa, and the wind is varied and weak, favorable for the accumulation of air pollutants in BTH. On January 15, the BTH is still controlled by the high pressure at the surface level and 850 hPa, and the westerly wind is prevailing at the 500 hPa. The weak surface wind, together with the stable stratification, further facilitates accumulation of air pollutants in the BTH. On January 16, a trough develops over the BTH at 850 hPa and 500 hPa, and the BTH is situated near the trough line, in which the northerly and southerly wind occurs at the same time. At the surface level, the northerly wind is prevailing in the north of BTH and the southerly wind is prevalent in the south of BTH, leading to evacuation of air pollutants in the north of BTH and the high level of air pollutants in the south of BTH. On January 17, the trough at 850 hPa commences to weaken and the controlling region of the trough at 500 hPa becomes narrow. The northwesterly wind is dominant over BTH, leading to divergence of the air pollutants in BTH. On January 18, the BTH is located near the ridgeline at 850hPa and at the verge of the high pressure at the surface level. The controlling scope of high-pressure system on the surface level is wide,

185 inducing the varied wind over the BTH and is not conductive to the evacuation of air
186 pollutants in BTH. On January 19, the prevailing southerly wind in the south of BTH and the
187 strong westerly wind in the west of BTH lead to the convergence of air pollutants at the
188 surface level. At 850 hPa and 500 hPa, BTH is situated in the southeast of the trough and
189 southwesterly wind is prevalent. On January 20, the BTH is located in the southwest of the
190 trough at 500 hPa and 850 hPa, and the strong northwesterly wind is prevailing over the BTH.
191 At the surface level, the BTH is situated between the high pressure in the west and the low
192 pressure in the east, inducing the strong northwesterly wind over BTH. The cold clean air
193 sweeps BTH and efficiently decreases the air pollutant concentrations in BTH.

194 **3.2 Uncertainties in Meteorological Simulations**

195 Figures 4a-d provide the temporal profiles of the ensemble simulations of the surface
196 meteorological fields and the corresponding observations at the meteorological site in Beijing
197 from 13 to 20 January 2014. The U component exhibits larger ensemble spread than the V
198 component (Figure s4), but the ensemble mean (ENSM) of the U component generally yields
199 the observed diurnal variations. The ensemble prediction of the V component fails to
200 reproduce the observed intensified southerly or northerly winds. The meteorological site is
201 located on the north of the Yanshan Mountains, substantially influenced by the mountain-
202 valley circulation (MVC). Apparently, the WRF-CHEM model lacks the ability to well
203 simulate the occurrence and development of MVC, causing the considerable biases of the
204 ensemble prediction of the V component. The ensemble prediction performs well in
205 producing the diurnal variation of the surface temperature, but the underestimation or
206 overestimation is still large when the V component prediction is biased. The relative
207 humidity (RH) shows a rather large ensemble spread (Figure s4d), and the ENSM reasonably
208 tracks the observed diurnal variation, with high nighttime and low afternoon simulated RH.
209 The RH simulation is sensitive to the simulated surface temperature. Generally, the

overestimation of the surface temperature well corresponds to the underestimation of the RH, or vice versa. The ENSM considerably overestimates the PBL height during daytime on January 13 and 14, and underestimates on January 15 (Figure 4e). In addition, most of the ensemble members frequently underestimate the observed PBL height during nighttime, and all ensemble members fail to produce the peak PBL height on January 17 and 20. The PBL height is principally determined by the vertical shear of horizontal winds and the ground thermal condition. Therefore, uncertainties of wind and temperature field simulations cause large biases of the PBL height simulation.

3.3 Uncertainties in Aerosol Species Simulations

Figure 5 shows the temporal profiles of the ensemble simulations of the aerosol species and the observations at IRSDE in Beijing. The ENSM reasonably produces the observed variations of the POA concentrations. However, all ensemble members fail to capture the peaks in the morning on January 16 and in the evening on January 17, indicating that the underestimation might not be caused by the meteorological uncertainties, but by emission biases. The POA in the atmosphere is from multiple sources, including the direct emissions from vehicles, cooking, biomass and coal combustion. Diurnal variations of those sources might constitute one of the major reasons for the biases of the POA simulations. The ENSM generally performs reasonably well in simulating the SOA concentration against the measured OOA. The ratio of the ensemble spread to the ensemble mean (RESM) for the SOA prediction is large compared to that of POA (Figures s5a, b). Four SOA formation pathways are included in simulations: oxidations of anthropogenic and biogenic volatile organic compounds (VOCs), oxidation HOA semi-volatile vapors, and irreversible uptake of glyoxal and methylglyoxal on aerosol surfaces. Therefore, uncertainties in meteorological fields not only influence the transport of the SOA precursors but also the SOA formation processes in the atmosphere, causing the rather large RESM of SOA simulations. The ENSM generally

235 reproduces the observed variations of sulfate, nitrate and ammonium (SNA), but the RESM
236 of SNA is also considerably large (Figures s5c-d). During haze days, sulfate is primarily
237 formed through heterogeneous reactions of SO_2 on aerosol surfaces, which is highly
238 dependent on the relative humidity (Li et al., 2017). Nitrate formation is determined by the
239 HNO_3 and N_2O_5 originated from the NO_2 oxidation, sensitive to the temperature and relative
240 humidity and also influenced by the level of sulfate in the particle phase and ammonia in the
241 atmosphere. The ammonium aerosol is formed through neutralization of sulfate and nitrate
242 aerosols by NH_3. Additionally, in the present study, ISORROPIA (Version 1.7) is used to
243 calculate the thermodynamic equilibrium between the sulfate-nitrate-ammonium-water
244 aerosols and their gas phase precursors H_2SO_4-HNO_3-NH_3-water vapor. Therefore,
245 uncertainties of meteorological fields propagate to the transport, atmospheric oxidation, and
246 thermal dynamic processes, which all have contributions to the large RESM of the SNA
247 simulations. Apparently, uncertainties in meteorological conditions substantially affect the
248 aerosol species simulations at a single observation site, which is consistent with the previous
249 studies (Bei et al., 2012).

250 **3.4 Uncertainties in $PM_{2.5}$ Simulations in BTH**

251 Heavy haze with high levels of $PM_{2.5}$ frequently constitutes a regional pollution event.
252 Figure 6 shows the temporal profiles of the ensemble simulations and observations of air
253 pollutants averaged at the monitoring sites in BTH from 13 to 20 January 2014. The RESM
254 of the average air pollutants is much less than those of aerosol species at the single
255 observation site (Figure s6). For the primary air pollutants, SO_2 and CO, the ENSM generally
256 tracks reasonably the observed variations. However, sometimes all the ensemble members
257 underestimate or overestimate the observation. There are two possible reasons for the biases
258 of ensemble simulations of SO_2 and CO: uncertainties of emissions and systematic errors of
259 meteorological fields. In the evening on January 15, the ensemble prediction substantially

overestimates the observed SO_2 concentration, but CO overestimation is not large. In the contrast, in the morning on January 16, the ensemble prediction slightly underestimates the SO_2 observation but remarkably underestimates the CO concentration. Therefore, the overestimation of SO_2 on January 15 and underestimation of CO on January 16 might be primarily contributed by the emission uncertainties. In the morning on January 18, the ensemble prediction significantly underestimates both SO_2 and CO observations, indicating the plausible uncertainties caused by the systematic errors of meteorological fields.

The ENSM of the average surface O_3 and NO_2 over the monitoring sites in BTH is in good agreement with observations. The ensemble prediction is subject to underestimate the O_3 observation during nighttime, but well consistent with the NO_2 observation. Considering the massive NO_x emission and the titration of NO, the nighttime O_3 concentrations are generally very low, particularly during wintertime when the daytime O_3 concentrations are not high. Hence, the underestimation of nighttime O_3 concentrations is perhaps caused by the observation uncertainties, such as the setting of lower detection limit. In addition, the ENSM does not reproduce the high O_3 level during nighttime on January 19 when the northwesterly wind is intensified to evacuate the air pollutants in BTH. Rapid increase of the observed O_3 concentrations during nighttime shows the substantial contribution of the background O_3 transport. Therefore, the background O_3 uncertainties constitute the major reason for the O_3 underestimation on January 19.

The ENSM also performs well in replicating the observed $PM_{2.5}$ observation, except the underestimation on January 16 and 18. However, the RESM of the $PM_{2.5}$ simulations is larger than those of O_3, NO_2, SO_2, and CO (Figure s6). The average ENSM of the $PM_{2.5}$ concentration over the monitoring sites during the simulation period is 189.5 $\mu g\ m^{-3}$, close to the observed 197.6 $\mu g\ m^{-3}$. In addition, the ensemble member of 16 and 30 (EN-16 and EN-30, respectively) produces the highest and lowest $PM_{2.5}$ level, with the average $PM_{2.5}$

285 concentrations of 231.5 and 167.3 μg m^{-3}, respectively. The $PM_{2.5}$ mainly include the primary
286 aerosols which are determined by direct emissions, and the secondary aerosols which are
287 determined by their precursors emissions and the homogeneous and heterogeneous oxidation
288 process in the atmosphere. Therefore, the large RESM of SOA and SNA simulations
289 enhances the ensemble spread of the $PM_{2.5}$ simulations.

290 Figure 7 presents the spatial distributions of ENSM and observations of the daily
291 average near-surface $PM_{2.5}$ mass concentrations during the haze episode, along with the
292 simulated wind fields. The ENSM predicted $PM_{2.5}$ spatial patterns are generally in good
293 agreement with the observations at the ambient monitoring sites in BTH. The ENSM
294 successfully reproduces the haze development and maturity stages from January 13 to 16,
295 2014. From January 17 to 18, the northeasterly wind develops and decreases the $PM_{2.5}$ level
296 in BTH, but not strong enough to evacuate the air pollutants. The $PM_{2.5}$ pattern of ENSM is
297 well consistent with observations, but on January 18, the $PM_{2.5}$ concentrations are remarkably
298 underestimated in four cities in BTH. On January 19, the westerly wind is prevailing in BTH,
299 causing the divergence of the $PM_{2.5}$. On January 20, the intensified northwesterly wind
300 commences to empty the $PM_{2.5}$ in BTH. However, apparently, the occurrence of the
301 intensification of the northwesterly wind is early, causing considerable underestimation of the
302 $PM_{2.5}$ concentration in the ENSM.

303 The uncertainties in meteorological fields are generally less than observational and
304 analysis errors, but the ensemble simulations still exhibit considerable spreads. In order to
305 contrast the $PM_{2.5}$ simulations of different ensemble members, we have selected two
306 members: EN-16 and EN-30, representing the highest and lowest $PM_{2.5}$ simulations in BTH,
307 respectively. Figure 8 provides the horizontal distributions of the daily average surface $PM_{2.5}$
308 concentrations along with surface winds during the episode in EN-16 and EN-30. Similar
309 $PM_{2.5}$ distribution patterns are simulated in EN-16 and EN-30, showing that the

meteorological uncertainties do not dominate the haze formation and development principally. The $PM_{2.5}$ level in EN-16 is much higher than that in EN-30 in BTH, which is mainly caused by the considerable discrepancies in the surface winds between the two members. The simulated southerly wind in EN-16 is generally more intense than that in EN-30, but the northerly wind in EN-16 is weak compared to EN-30, which is more favorable for the air pollutants accumulation in EN-16 than EN-30. On January 13 and 14, the winds in EN-30 are weak or calm in BTH and the $PM_{2.5}$ is mainly attributed to the local production. However, in EN-16, the prevailing south winds also deliver the air pollutants from the south areas to BTH, substantially enhancing the $PM_{2.5}$ level. On January 15, although EN-16 and EN-30 both produce the prevailing southerly wind in BTH, the westerly wind in EN-30 is intense compared to EN-16, considerably decreasing the $PM_{2.5}$ level in EN-30. On January 16, the northeasterly wind in EN-30 is intensified and evacuates the $PM_{2.5}$ in the north of BTH. However, in EN-16, the simulated northeasterly wind is weak and the $PM_{2.5}$ level in the north of BTH still remains high. On January 17, the simulated northerly wind in EN-16 is weak compared to that in EN-30, causing higher $PM_{2.5}$ concentration in EN-16 than EN-30 in BTH. On January 18, the intensified southerly wind in EN-16 considerably increases the $PM_{2.5}$ level in BTH compared to EN-30. On January 19, the westerly wind is prevalent in EN-30 and the $PM_{2.5}$ level commences to decrease, but in EN-16, the southwesterly wind still causes high $PM_{2.5}$ concentrations in BTH. On January 20, the stronger northeasterly wind in EN-30 more efficiently evacuates the $PM_{2.5}$ than that in EN-16.

3.5 Uncertainties in $PM_{2.5}$ Simulations in Mega-cities

EN-16 and EN-30 both predict the haze occurrence and development in BTH during the episode, although the difference of the $PM_{2.5}$ level between those two members is considerable, showing that the meteorological uncertainties do not dominate the regional haze formation. Previous studies have shown that the meteorological uncertainties

335 substantially impact the air quality simulations at the city-scale (Bei et al., 2012). Figure 10
336 presents the temporal variation of the ensemble simulations and observations averaged at four
337 mega-cities in BTH during the episode. The ENSM of the $PM_{2.5}$ concentrations in Beijing,
338 Tianjin, and Baoding is in good agreement with the observation. However, the ENSM
339 remarkably underestimates the observed $PM_{2.5}$ concentration in Shijiazhuang from January
340 16 to 19, which is hardly interpreted by the emission biases. The ENSM performs well in
341 simulating the $PM_{2.5}$ variations from January 13 to 15, and overestimates the observation on
342 January 20 in Shijiazhuang. One of the possible reasons for the underestimation in
343 Shijiazhuang is that the westerly wind is systematically overestimated from January 16 to 19
344 along the foothills of the Taihang Mountains, causing the haze plume to move eastwardly.
345 Although the ENSM produces reasonably well the $PM_{2.5}$ variations in the four mega-
346 cities against the measurement, the meteorological uncertainties still cause large uncertainties
347 of the $PM_{2.5}$ concentration (Figure s7). During the first three days of the episode, the ENSM
348 is well consistent with the observations in the four mega-cites, but the $PM_{2.5}$ level
349 discrepancy between the members with the highest and lowest $PM_{2.5}$ concentrations is rather
350 large, causing troubles for the assessment of the control strategies. For example, in
351 Shijiazhuang, the average $PM_{2.5}$ concentrations during the first three days in the members
352 with the highest and lowest $PM_{2.5}$ concentrations are 403.5 and 213.8 $\mu g\ m^{-3}$, respectively,
353 and the difference is about 190 $\mu g\ m^{-3}$. In Beijing, the average $PM_{2.5}$ concentrations in the
354 two members are 103.9 and 196.3 $\mu g\ m^{-3}$. It is worth noting that, according to the Chinese air
355 quality standard released in 2012, the $PM_{2.5}$ concentration of 103.9 $\mu g\ m^{-3}$ is defined as
356 “lightly polluted condition”, but 196.3 $\mu g\ m^{-3}$ defined as “heavily polluted condition”. If the
357 heavy air pollution occurs, the control strategies will be implemented. Therefore, it is
358 necessary to use the ensemble simulation to avoid the impact of the meteorological
359 uncertainties on the haze prediction.

4 Summary and Conclusions

In the present study, the uncertainties in simulating haze formation due to meteorological uncertainties are investigated using the WRF-CHEM model through ensemble simulations. A persistent heavy haze episode occurred in BTH from 13 to 20 is simulated. A climatological ensemble initialization approach is used to produce initial and boundary conditions for each ensemble member.

The ENSMs of the aerosol constituents are generally in good agreement with the observations at an observation site in Beijing, including the sharp buildup of the aerosol constituents in the evening on January 15 and rapid falloff in the morning on January 20. However, the ENSM considerably underestimates the observed primary aerosols in the evening on January 17. The ensemble spread is rather large for the aerosol constituent simulations, and the RESM exceeds 50%, respectively.

The ENSM performs well in simulating the temporal variations of the average surface CO, SO_2, NO_2, O_3 and $PM_{2.5}$ mass concentrations over the monitoring sites in BTH, and the RESM of the air pollutants is generally less than 30%. The RESM of $PM_{2.5}$ simulations is larger than the other air pollutants, which is due to the complicated composition of $PM_{2.5}$, including the contributions of primary and secondary aerosols. The meteorological uncertainties do not principally dominate the haze formation and development, but considerably alter the simulated $PM_{2.5}$ level. The average $PM_{2.5}$ difference during the episode exceeds 60 μg m^{-3} between the two members with the highest and lowest $PM_{2.5}$ simulations.

Although the meteorological uncertainties do not dominate the regional haze formation, they still substantially influence the $PM_{2.5}$ simulations at city-scale. The ENSM reasonably well predicts the $PM_{2.5}$ variations in the four mega-cities against the measurements, including Beijing, Tianjin, Baoding and Shijiazhuang, but the RESM of the $PM_{2.5}$ simulations is rather

large, causing troubles for the evaluation of the control strategies. Therefore, the ensemble simulation is needed to take into consideration the impact of the meteorological uncertainties on the haze prediction. It is worth noting that aside from meteorological fields, uncertainties in emissions or various chemistry/aerosol schemes also considerably influence the WRF-CHEM model simulations. The extended response surface modeling (ERSM) technique can be used to quantify the relative importance of each uncertainty source in the WRF-CHEM model (Zhao et al, 2017).

Acknowledgement: Naifang Bei is supported by the National Natural Science Foundation of China (no. 41275101 and no. 41430424) and the Fundamental Research Funds for the Central Universities of China. Guohui Li is supported by "Hundred Talents Program" of the Chinese Academy of Sciences and the National Natural Science Foundation of China (no. 41661144020). This work is financially supported by National Key R&D Plan (Quantitative Relationship and Regulation Principle between Regional Oxidation Capacity of Atmospheric and Air Quality (2017YFC0210000)).

406 **References**

407 Beekmann, M. and Derognat, C.: Monte Carlo uncertainty analysis of a regional-scale
408 chemistry model constrained by measurements from the Atmospheric Pollution Over the
409 Paris Area (ESQUIF) campaign, J. Geophys. Res., 108, 8559,
410 doi:10.1029/2003JD003391, 2003.

411 Bei, N., de Foy, B., Lei, W., Zavala, M., and Molina, L. T.: Using 3DVAR data assimilation
412 system to improve ozone simulations in the Mexico City basin, Atmos. Chem. Phys., 8,
413 7353-7366, 2008.

414 Bei, N., Lei, W., Zavala, M., and Molina, L. T.: Ozone predictabilities due to meteorological
415 uncertainties in the Mexico City basin using ensemble forecasts, Atmos. Chem. Phys., 10,
416 6295–6309, doi:10.5194/acp-10-6295-2010, 2010.

417 Bei, N., Li, G., and Molina, L. T.: Uncertainties in SOA simulations due to meteorological
418 uncertainties in Mexico City during MILAGRO-2006 field campaign, Atmos. Chem.
419 Phys., 12, 11295–11308, doi:10.5194/acp-12-11295-2012, 2012.

420 Bei, N., Li, G., Huang, R., Cao, J., Meng, N., Feng, T., Liu, S., Zhang, T., Zhang, Q., and
421 Molina, L. T.: Typical synoptic situations and their impacts on the wintertime air
422 pollution in the Guanzhong basin, China, Atmos. Chem. Phys., 16, 7373–7387, 2016a.

423 Bei, N., Xiao, B., Meng, N., and Feng, T.: Critical role of meteorological conditions in a
424 persistent haze episode in the Guanzhong basin, China, Sci. Total Environ., 550, 273–284,
425 2016b.

426 Binkowski, F. S. and Roselle, S. J.: Models-3 Community Multiscale Air Quality (CMAQ)
427 model aerosol component: 1. Model description, J. Geophys. Res., 108, 4183,
428 doi:10.1029/2001JD001409, 2003.

429 Chan, C. K., and Yao, X.: Air pollution in mega cities in China, Atmos. Environ., 42, 1–42,
430 2008.

431 Chen, F., and Dudhia, J.: Coupling an advanced land surface-hydrology model with the Penn
432 State-NCAR MM5 modeling system. Part I: Model implementation and sensitivity, Mon.
433 Weather Rev., 129, 569-585, 10.1175/1520-0493(2001) 129<0569:caalsh>2.0.co; 2, 2001.

434 Chou, M. D., and Suarez, M. J.: A solar radiation parameterization for atmospheric studies,
435 NASA TM-104606, Nasa Tech.memo, 15, 1999.

436 Chou, M. D., Suarez, M. J., Liang, X. Z., Yan, M. H., and Cote, C.: A Thermal Infrared
437 Radiation Parameterization for Atmospheric Studies, Max J, 2001.

438 Canonaco, F., Crippa, M., Slowik, J. G., Baltensperger, U., and Prevot, A. S. H.: SoFi, an
439 IGOR-based interface for the efficient use of the generalized multilinear engine (ME-2)
440 for the source apportionment: ME-2 application to aerosol mass spectrometer data, Atmos.
441 Meas. Tech., 6(12), 3649–3661, 2013

442 Delle Monache, L. and Stull, R.: An ensemble air quality forecast over western Europe
443 during an ozone forecast, Atmos. Environ., 37, 3469–3474, 2003.

444 Delle Monache, L., Deng, X., Zhou, Y., and Stull, R.: Ozone ensemble forecasts: A new
445 ensemble design, J. Geophys. Res., 111, D05307, doi:10.1029/2005JD006310, 2006.

446 Dabberdt, W. F., Carroll, M. A., Baumgardner, D., Carmichael, G., Cohen, R., Dye, T., Ellis,
447 J., Grell, G., Grimmond, S., Hanna, S., Irwin, J., Lamb, B., Madronich, S., Mcqueen, J.,
448 Meagher, J., Odman, T., Pleim, J., Schmid, H. P., and Westphal, D. L.: Meteorological
449 research needs for improved air quality forecasting: Report of the 11th Prospectus

Development Team of the U.S. Weather Research Program, B. Am. Meteorol. Soc., 85, 563–586, 2004.

Dabberdt, W. F. and Miller E.: Uncertainty, ensembles and air quality dispersion modeling: Applications and challenges, Atmos. Environ., 34, 4667–4673, 2000.

Elser, M., Huang, R.-J., Wolf, R., Slowik, J. G., Wang, Q., Canonaco, F., Li, G., Bozzetti, C., Daellenbach, K. R., Huang, Y., Zhang, R., Li, Z., Cao, J., Baltensperger, U., El-Haddad, I., and Prévôt, A. S. H.: New insights into $PM_{2.5}$ chemical composition and sources in two major cities in China during extreme haze events using aerosol mass spectrometry, Atmos. Chem. Phys., 16, 3207–3225, https://doi.org/10.5194/acp-16-3207-2016, 2016

Fang, M., Chan, C. K., and Yao, X. H.: Managing air quality in a rapidly developing nation: China, Atmos. Environ., 43, 79–86, 2009.

Feng, T., Li, G., Cao, J., Bei, N., Shen, Z., Zhou, W., Liu, S., Zhang, T., Wang, Y., Huang, R.-J., Tie, X., and Molina, L. T.: Simulations of organic aerosol concentrations during springtime in the Guanzhong Basin, China, Atmos. Chem. Phys., 16, 10045–10061, https://doi.org/10.5194/acp-16-10045-2016, 2016.

Galmarini, S., Bianconi, R., Klug, W., Mikkelsen, T., Addis, R., An- dronopoulos, S., Astrup, P., Baklanov, A., Bartniki, J., Bartzis, J. C., Bellasio, R., Bompay, F., Buckley, R., Bouzom, M., Champion, H., D'Amours, R., Davakis, E., Eleveld, H., Geertsema, G. T., Glaab, H., Kollax, M., Ilvonen, M., Manning, A., Pechinger, U., Persson, C., Polreich, E., Potemski, S., Prodanova, M., Salt- bones, J., Slaper, H., Sofiev, M. A., Syrakov, D., Sørensen, J. H., Van der Auwera, L., Valkama, I., and Zelazny, R.: Ensemble dispersion forecasting – Part I: Concept, approach and indicators, Atmos. Environ., 38, 4607–4617, 2004.

Gao, Y., Liu, X., Zhao, C., and Zhang, M.: Emission controls versus meteorological conditions in determining aerosol concentrations in Beijing during the 2008 Olympic Games, Atmos. Chem. Phys., 11, 12437–12451, doi:10.5194/acp-11-12437-2011, 2011.

Guenther, A., Karl, T., Harley, P., Wiedinmyer, C., Palmer, P. I., and Geron, C.: Estimates of global terrestrial isoprene emissions using MEGAN (Model of Emissions of Gases and Aerosols from Nature), Atmos. Chem. Phys., 6, 3181–3210, doi:10.5194/acp-6-3181-2006, 2006.

Guo, S., M. Hu, M. L. Zamora, J. Peng, D. Shang, J. Zheng, Z. Du, Z. Wu, M. Shao, L. Zeng, M. J. Molina, and R. Zhang: Elucidating severe urban haze formation in China, P. Natl. Acad. Sci. USA, 111, 17373–17378, 2014.

Hong, S.-Y., Dudhia, J., and Chen, S.-H.: A revised approach to ice microphysical processes for the bulk parameterization of clouds and precipitation, Mon. Wea. Rev., 132, 103–120, 2004.

Horowitz, L. W., Waters, S., Mauzerall, D. L., Emmons, L. K., Rasch, P. J., Tie, X., Lamarque, J.-F., Schultz, M. G., Tyndall, G. S., Orlando, J. J., and Brasseur, G. P.: A global simulation of tropospheric ozone and related tracers: Description and evaluation of MOZART, version 2, J. Geophys. Res., 108, 4784, doi:10.1029/2002JD002853, 2003.

Huang, R. J., Zhang, Y. L., Bozzetti, C., Ho, K. F., Cao, J. J., Han, Y. M., Dällenbach, K. R., Slowik, J. G., Platt, S. M., Canonaco, F., Zotter, P., Wolf, R., Pieber, S. M., Bruns, E. A., Crippa, M., Ciarelli, G., Piazzalunga, A., Schwikowski, M., Abbaszade, G., Schnelle-Kreis, J., Zimmermann, R., An, Z. S., Szidat, S., Baltensperger, U., EI Haddad, I., Prévôt,

494 A. S. H.: High secondary aerosol contribution to particulate pollution during haze events
495 in China, Nature, 514, 218–222, 2014.

496 Janjic, Z. I.: Nonsingular implementation of the Mellor-Yamada level 2.5 scheme in the
497 NCEP Meso Model, NCEP Office Note, 437, 61 pp., 2002.

498 Li, G., Lei, W., Zavala, M., Volkamer, R., Dusanter, S., Stevens, P., Molina, L.T.: Impacts of
499 HONO sources on the photochemistry in Mexico City during the MCMA-2006/MILAGO
500 Campaign, Atmos. Chem. Phys., 10, 6551–6567, 2010.

501 Li, G., Bei, N., Tie, X., and Molina, L. T.: Aerosol effects on the photochemistry in Mexico
502 City during MCMA-2006/MILAGRO campaign, Atmos. Chem. Phys., 11, 5169–5182,
503 10.5194/acp-11-5169-2011, 2011a.

504 Li, G., Zavala, M., Lei, W., Tsimpidi, A. P., Karydis, V. A., Pandis, S. N., Canagaratna, M.
505 R., and Molina, L. T.: Simulations of organic aerosol concentrations in Mexico City using
506 the WRF-CHEM model during the MCMA-2006/MILAGRO campaign, Atmos. Chem.
507 Phys., 11, 3789–3809, 10.5194/acp-11-3789-2011, 2011b.

508 Li, G., Lei, W., Bei, N., and Molina, L. T.: Contribution of garbage burning to chloride and
509 $PM_{2.5}$ in Mexico City, Atmos. Chem. Phys., 12, 8751–8761, 10.5194/acp-12-8751-2012,
510 2012.

511 Li, G., Bei, N., Cao, J., Huang, R., Wu, J., Feng, T., Wang, Y., Liu, S., Zhang, Q., and Tie, X.:
512 A possible pathway for rapid growth of sulfate during haze days in China, Atmos. Chem.
513 Phys., 17, 1-43, 2017.

514 Li, G., Bei, N., Cao, J., Wu, J., Long, X., Feng, T., Dai, W., Liu, S., Zhang, Q., and Tie, X.:
515 Widespread and persistent ozone pollution in eastern China during the non-winter season
516 of 2015: observations and source attributions, Atmos. Chem. Phys., 17, 2759–2774,
517 doi:10.5194/acp-17-2759-2017, 2017.

518 Liu, T., Gong, S., He, J., Yu, et al.: Attributions of meteorological and emission factors to the
519 2015 winter severe haze pollution episodes in China's Jing-Jin-Ji area, Atmos. Chem.
520 Phys., 17, 2971–2980, doi:10.5194/acp-17-2971-2017, 2017.

521 Mallet, V. and Sportisse, B.: Ensemble-based air quality forecasts: A multi-model approach
522 applied to ozone, J. Geophys. Res., 111, D18302, doi:10.1029/2005JD006675, 2006.

523 Menut, L.: Adjoint modeling for atmospheric pollution process sensitivity at regional scale, J.
524 Geophys. Res., 108, 8562, doi:10.1029/2002JD002549, 2003.

525 McKeen, S., Wilczak, J., Grell, G., Djalalova, I., Peckham, S., Hsie, E.-Y., Gong, W.,
526 Bouchet, V., Menard, S., Moffet, R., McHenry, J., McQueen, J., Tang, Y., Carmichael, G.
527 R., Pagowski, M., Chan, A., Dye, T., Frost, G., Lee, P., and Mathur, R: Assessment of an
528 ensemble of seven realtime ozone forecasts over eastern North America during the
529 summer of 2004, J. Geophys. Res., 110, D21307, doi:10.1029/2005JD005858, 2005.

530 Nenes, A., Pandis, S. N., and Pilinis, C.: ISORROPIA: A new thermodynamic equilibrium
531 model for multiphase multicomponent inorganic aerosols, Aquat. Geochem., 4, 123–152,
532 10.1023/a:1009604003981, 1998.

533 Penner, J. E. et al. Aerosols, their direct and indirect effects, in: Climate Change 2001: The
534 Scientific Basis, Contributions of Working Group I to the Third Assessment Report of the
535 Intergovernmental Panel on Climate Change, edited by: Houghton, J. T., Ding, Y., Griggs,
536 D. J., Noguer, M., van der Linden, P. J., Dai, X., Maskell K., and Johnson, C. A.,
537 Cambridge University Press, Cambridge, UK, and New York, NY, USA, 289–348, 2001.

Pope III, C. A. and Dockery, D. W.: Health effects of fine particulate air pollution: Liens that connect, J. Air. Waste Manage, 56, 709–742, 2006.

Sharma, A., Ojha, N., Pozzer, A., Mar, K. A., Beig, G., Lelieveld, J., and Gunthe, S., WRF-Chem simulated surface ozone over South Asia during the pre-monsoon: Effects of emission inventories and chemical mechanisms, Atmos. Chem. Phys. Discuss., doi:10.5194/acp-2016-1083, in review, 2016.

Nielsen-Gammon, J. W., McNider, R. T., Angevine, W. M., White, A. B., and Knupp, K.: Mesoscale model performance with assimilation of wind profiler data: Sensitivity to assimilation parameters and network configuration. J. Geophys. Res., 112, D09119, doi:10.1029/2006JD007633, 2007.

Solazzo, E., Bianconi, R., Hogrefe, C., Curci, G., Tuccella, P., Alyuz, U., Balzarini, A., Baró, R., Bellasio, R., Bieser, J., Brandt, J., Christensen, J. H., Colette, A., Francis, X., Fraser, A., Vivanco, M. G., Jiménez-Guerrero, P., Im, U., Manders, A., Nopmongcol, U., Kitwiroon, N., Pirovano, G., Pozzoli, L., Prank, M., Sokhi, R. S., Unal, A., Yarwood, G., and Galmarini, S.: Evaluation and error apportionment of an ensemble of atmospheric chemistry transport modeling systems: multivariable temporal and spatial breakdown, Atmos. Chem. Phys., 17, 3001–3054, https://doi.org/10.5194/acp-17-3001-2017, 2017.

Wang, H., Xu, J., Zhang, M., Yang, Y., Shen, X., Wang, Y., Chen, D., Guo, J.: A study of the meteorological causes of a prolonged and severe haze episode in January 2013 over central-eastern China, Atmos. Environ., 98, 146–157, 2014.

Williams, L. R., Gonzalez, L. A., Peck, J., Trimborn, D., McInnis, J., Farrar, M. R., Moore, K. D., Jayne, J. T., Robinson, W. A., Lewis, D. K., Onasch, T. B., Canagaratna, M. R., Trimborn, A., Timko, M. T., Magoon, G., Deng, R., Tang, D., Blanco, E., Prevot, A. S. H., Smith, K. A., and Worsnop, D. R.: Characterization of an aerodynamic lens for transmitting particles greater than 1 micrometer in diameter into the Aerodyne aerosol mass spectrometer, Atmos. Meas. Tech., 6(11), 3271–3280, 2013.

Wu, J., Li, G., Cao, J., Bei, N., Wang, Y., Feng, T., Huang, R., Liu, S., Zhang, Q., and Tie, X.: Contributions of trans-boundary transport to summertime air quality in Beijing, China, Atmos. Chem. Phys., 17, 2035–2051, doi:10.5194/acp-17-2035-2017, 2017.

Wu, M., Wu, D., Fan, Q., Wang, B. M., Li, H. W., and Fan, S. J.: Observational studies of the meteorological characteristics associated with poor air quality over the Pearl River Delta in China, Atmos. Chem. Phys., 13, 10755–10766, doi:10.5194/acp-13-10755-2013, 2013.

Zhang, F., Bei, N., Nielsen-Gammon, J. W., Li, G., Zhang, R., Stuart, A. L., and Aksoy, A.: Impacts of meteorological uncertainties on ozone pollution predictability estimated through meteorological and photochemical ensemble forecasts, J. Geophys. Res., 112, D04304, doi:10.1029/2006JD007429, 2007.

Zhang, J. P., Zhu, T., Zhang, Q. H., Li, C. C., Shu, H. L., Ying, Y., Dai, Z. P., Wang, X., Liu, X. Y., Liang, A. M., Shen, H. X., and Yi, B. Q.: Impact of circulation patterns on transport paths and air quality, Atmos. Chem. Phys., 12, 5031–5053, 2012.

Zhang, Q., Streets, D. G., Carmichael, G. R., He, K. B., Huo, H., Kannari, A., Klimont, Z., Park, I. S., Reddy, S., Fu, J. S., Chen, D., Duan, L., Lei, Y., Wang, L. T., and Yao, Z. L.: Asian emissions in 2006 for the NASA INTEX-B mission, Atmos. Chem. Phys., 9, 5131–5153, 2009.

Zhang, Q., Quan, J., Tie, X., Li, X., Liu, Q., Gao, Y., and Zhao, D.: Effects of meteorology and secondary particle formation on visibility during heavy haze events in Beijing, China, Sci. Total Environ., 502, 578–584, 2015.

584 Zhang, R., Li, G., Fan, J., Wu, D. L., and Molina, M. J.: Intensification of Pacific storm track
585 linked to Asian pollution, P. Natl. Acad. Sci. USA, 104, 5295–5299, 2007.

586 Zhao, B., Wu, W., Wang, S., Xing, J., Chang, X., Liou, K.-N., Jiang, J. H., Gu, Y., Jang, C.,
587 Fu, J. S., Zhu, Y., Wang, J., Lin, Y., and Hao, J.: A modeling study of the nonlinear
588 response of fine particles to air pollutant emissions in the Beijing–Tianjin–Hebei region,
589 Atmos. Chem. Phys., 17, 12031-12050, https://doi.org/10.5194/acp-17-12031-2017, 2017.

590 Zhao, X. J., Zhao, P. S., Xu, J., Meng, W., Pu, W. W., Dong, F., He, D., and Shi, Q. F.:
591 Analysis of a winter regional haze event and its formation mechanism in the North China
592 Plain, Atmos. Chem. Phys., 13, 5685–5696, 2013.

593
594

Figure Captions

Figure 1 WRF-CHEM simulation domain. The filled red (in BTH) and blue (outside of BTH) circles represent centers of cities with ambient monitoring site. The size of the circle denotes the number of ambient monitoring sites of cities. The filled black triangle and rectangle denote the deployment location of the HR-ToF-AMS and the surface meteorological site in Beijing.

Figure 2 Vertical distribution of the mean of initial ensemble spreads and the standard deviation for (a) horizontal winds (U and V components), (b) temperature, (c) pressure, and (d) water vapor mixing ratio.

Figure 3 Observed hourly $PM_{2.5}$ concentrations averaged in (a) four megacities cities (including Beijing, Tianjin, Baoding, and Shijiazhuang) and (b) nine non-megacities of BTH during the period from January 13 to 20, 2014.

Figure 4 Temporal evolution of the surface (a) U component, (b) V component, (c) temperature, and (d) relative humidity at the meteorological site, and (e) the PBL height at IRSDE in Beijing from each ensemble member (thin green lines), the ensemble mean (bold black line), and observations (black dots) from January 13 to 20, 2014.

Figure 5 Temporal evolution of the (a) POA, (b) SOA, (c) sulfate, (d) nitrate, and (e) ammonium mass concentrations at IRSDE in Beijing from each ensemble member (thin green lines), the ensemble mean (bold black line), and observations (black dots) from January 13 to 20, 2014.

Figure 6 Temporal evolution of the (a) $PM_{2.5}$, (b) O_3, (c) NO_2, (d) SO_2, and (e) CO mass concentrations averaged over monitoring sites in BTH from each ensemble member (thin green lines), the ensemble mean (bold black line), and observations (black dots) from January 13 to 20, 2014.

Figure 7 ENSM of the daily average surface $PM_{2.5}$ concentration distributions (color contour) along with the ENSM of the daily average surface winds (black arrows) from January 13 to 20, 2014. The colored circles denote the $PM_{2.5}$ measurements in cities.

Figure 8 Same as Figure 7, but for the ensemble member of 16 with the highest simulated $PM_{2.5}$ concentration.

Figure 9 Same as Figure 7, but for the ensemble member of 30 with the lowest simulated $PM_{2.5}$ concentration.

Figure 10 Temporal evolution of the $PM_{2.5}$ mass concentrations averaged in (a) Beijing, (b) Tianjin, (c) Baoding, and (d) Shijiazhuang from each ensemble member (thin green lines), the ensemble mean (bold black line), and observations (black dots) during the period from January 13 to 20, 2014. The red and blue lines represent the simulations in the members with highest and lowest $PM_{2.5}$ concentrations, respectively.

638 Table 1 WRF-CHEM model configurations
639

Regions	**Beijing-Tianjin-Hebei (BTH)**
Simulation period	January 13 to 21, 2014
Domain size	200 × 200
Domain center	39°N, 117°E
Horizontal resolution	6km × 6km
Vertical resolution	35 vertical levels with a stretched vertical grid with spacing ranging from 30 m near the surface, to 500 m at 2.5 km and 1 km above 14 km
Microphysics scheme	WSM 6-class graupel scheme (Hong and Lim, 2006)
Boundary layer scheme	MYJ TKE scheme (Janjić, 2002)
Surface layer scheme	MYJ surface scheme (Janjić, 2002)
Land-surface scheme	Unified Noah land-surface model (Chen and Dudhia, 2001)
Longwave radiation scheme	Goddard longwave scheme (Chou and Suarez, 2001)
Shortwave radiation scheme	Goddard shortwave scheme (Chou and Suarez, 1999)
Meteorological boundary and initial conditions	NCEP 1°×1° reanalysis data
Chemical initial and boundary conditions	MOZART 6-hour output (Horowitz et al., 2003)
Anthropogenic emission inventory	Developed by Zhang et al. (2009)
Biogenic emission inventory	MEGAN model developed by Guenther et al. (2006)

640
641
642
643
644

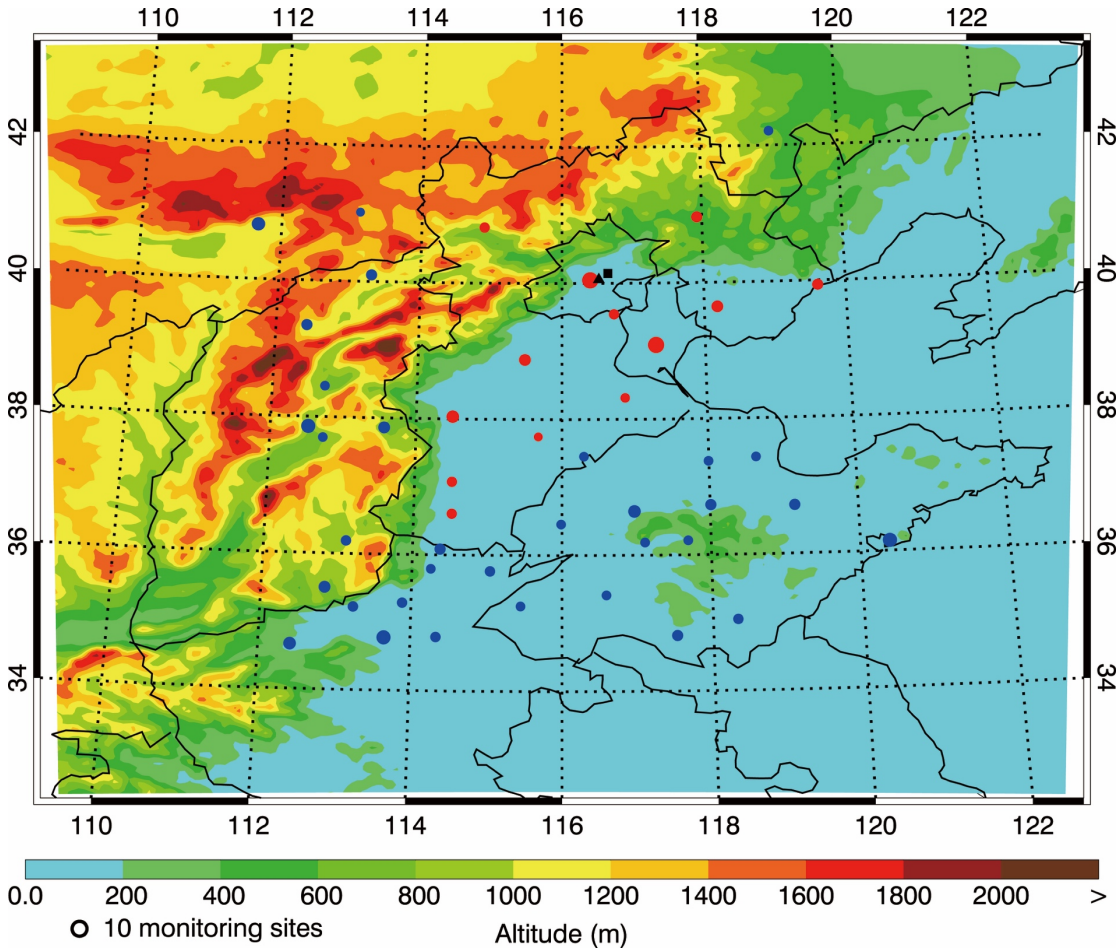

Figure 1 WRF-CHEM simulation domain. The filled red (in BTH) and blue (outside of BTH) circles represent centers of cities with ambient monitoring site. The size of the circle denotes the number of ambient monitoring sites of cities. The filled black triangle and rectangle denote the deployment location of the HR-ToF-AMS and the surface meteorological site in Beijing.

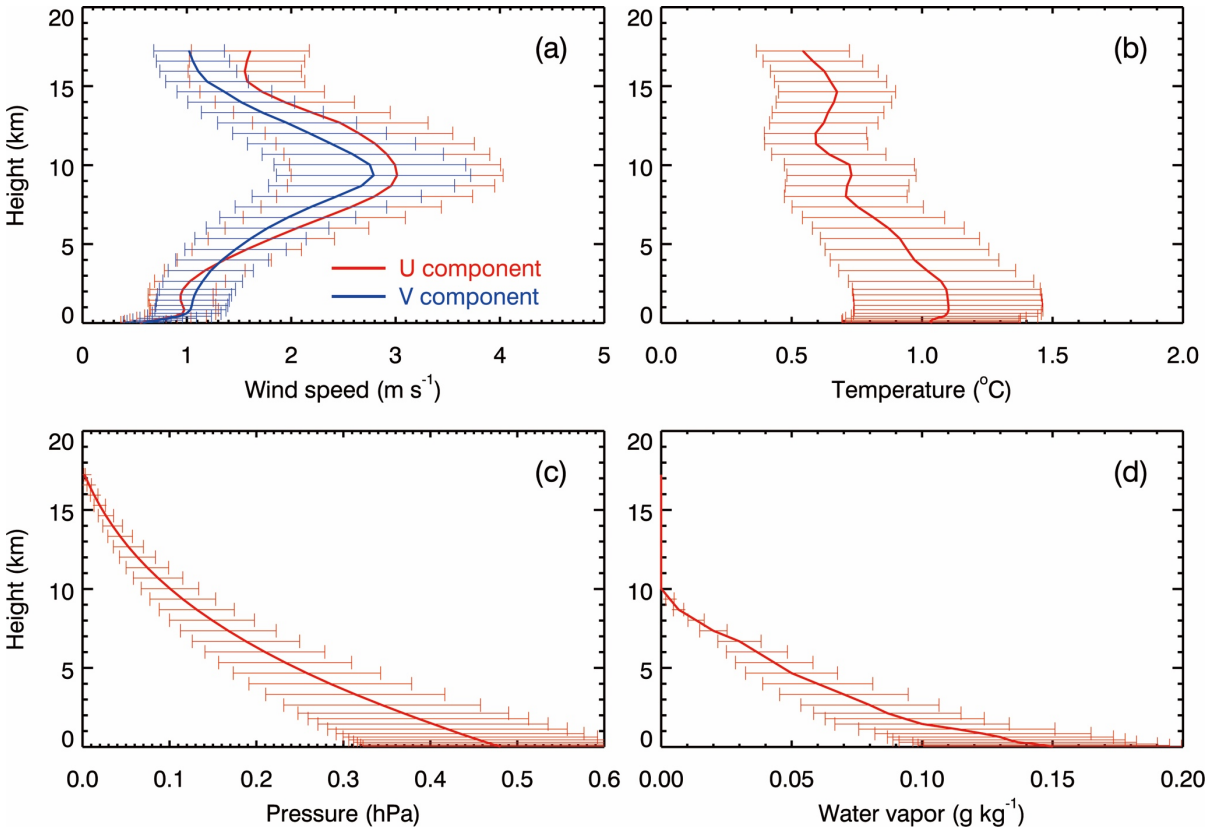

Figure 2 Vertical distribution of the mean of initial ensemble spreads and the standard deviation for (a) horizontal winds (U and V components), (b) temperature, (c) pressure, and (d) water vapor mixing ratio.

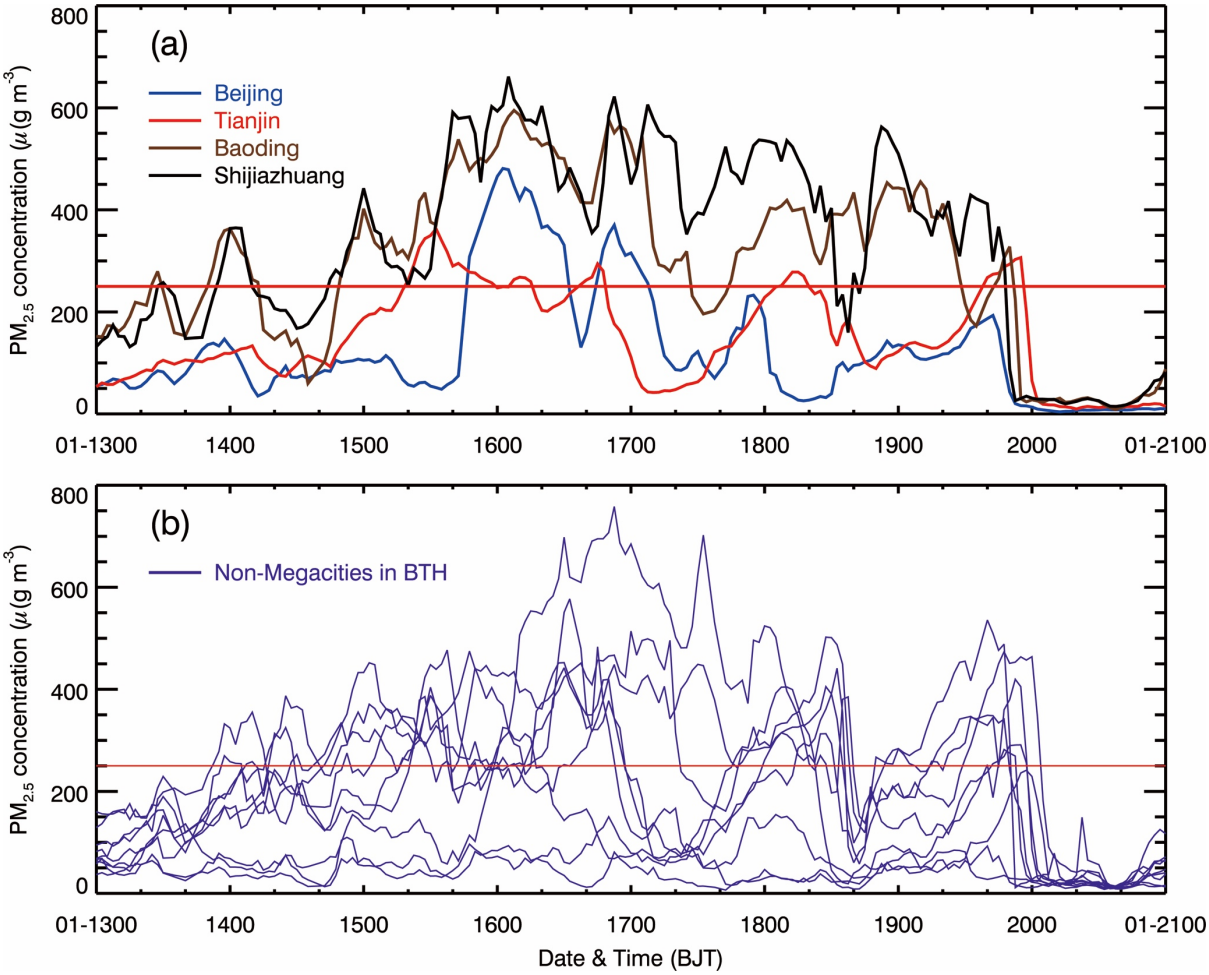

Figure 3 Observed hourly $PM_{2.5}$ concentrations averaged in (a) four megacities cities (including Beijing, Tianjin, Baoding, and Shijiazhuang) and (b) nine non-megacities of BTH during the period from January 13 to 20, 2014.

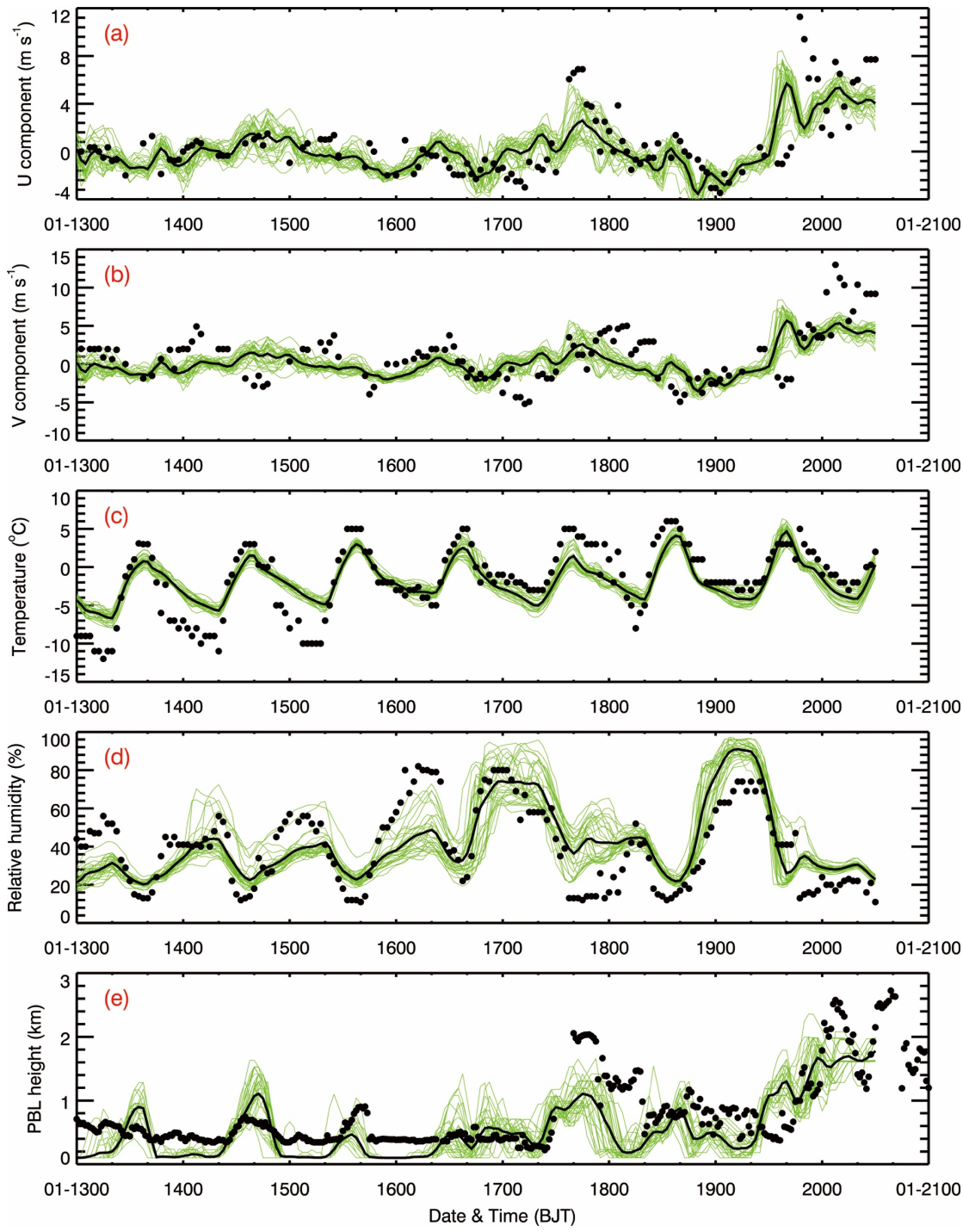

Figure 4 Temporal evolution of the surface (a) U component, (b) V component, (c) temperature, and (d) relative humidity at the meteorological site, and (e) the PBL height at IRSDE in Beijing from each ensemble member (thin green lines), the ensemble mean (bold black line), and observations (black dots) from January 13 to 20, 2014.

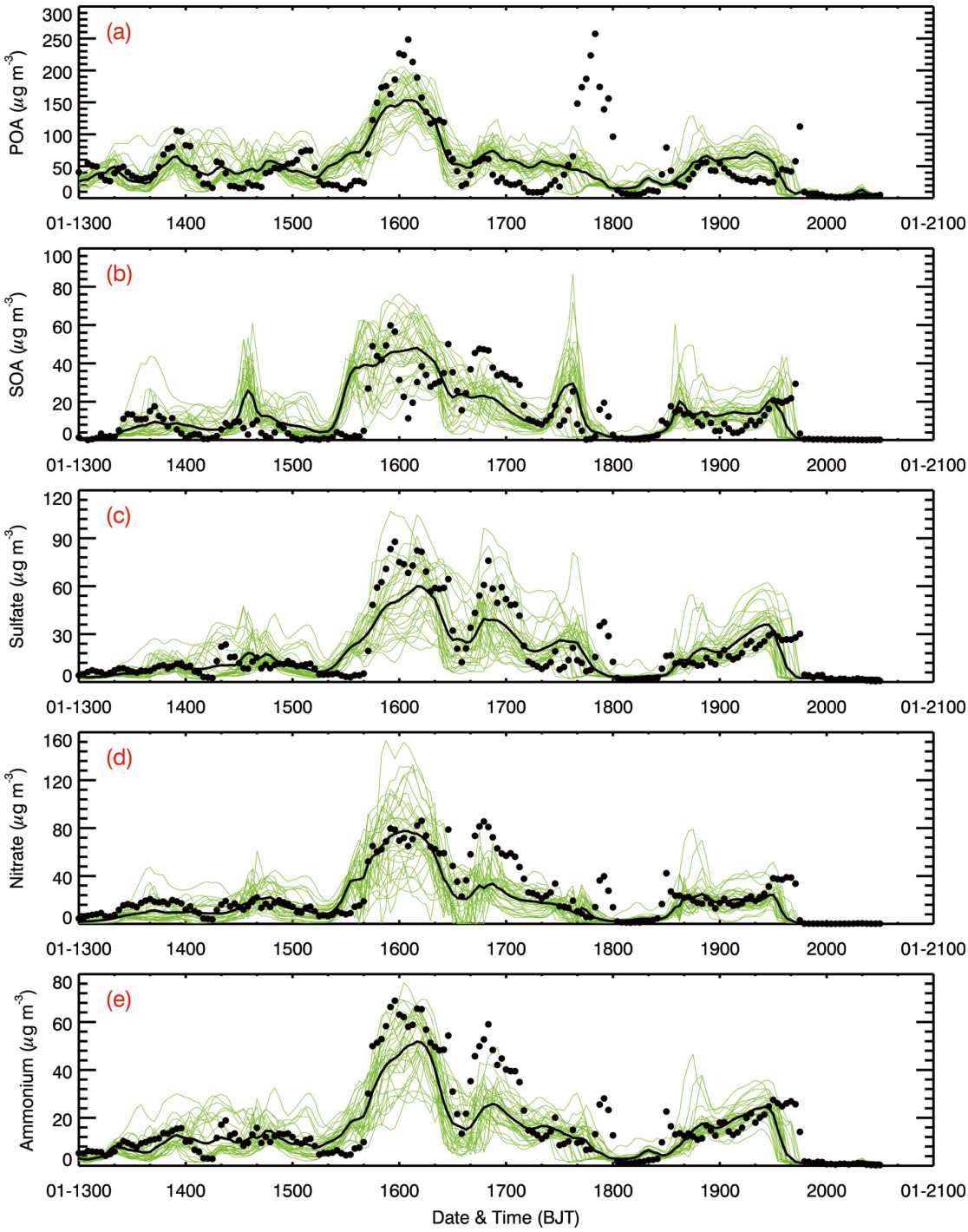

Figure 5 Temporal evolution of the (a) POA, (b) SOA, (c) sulfate, (d) nitrate, and (e) ammonium mass concentrations at IRSDE in Beijing from each ensemble member (thin green lines), the ensemble mean (bold black line), and observations (black dots) from January 13 to 20, 2014.

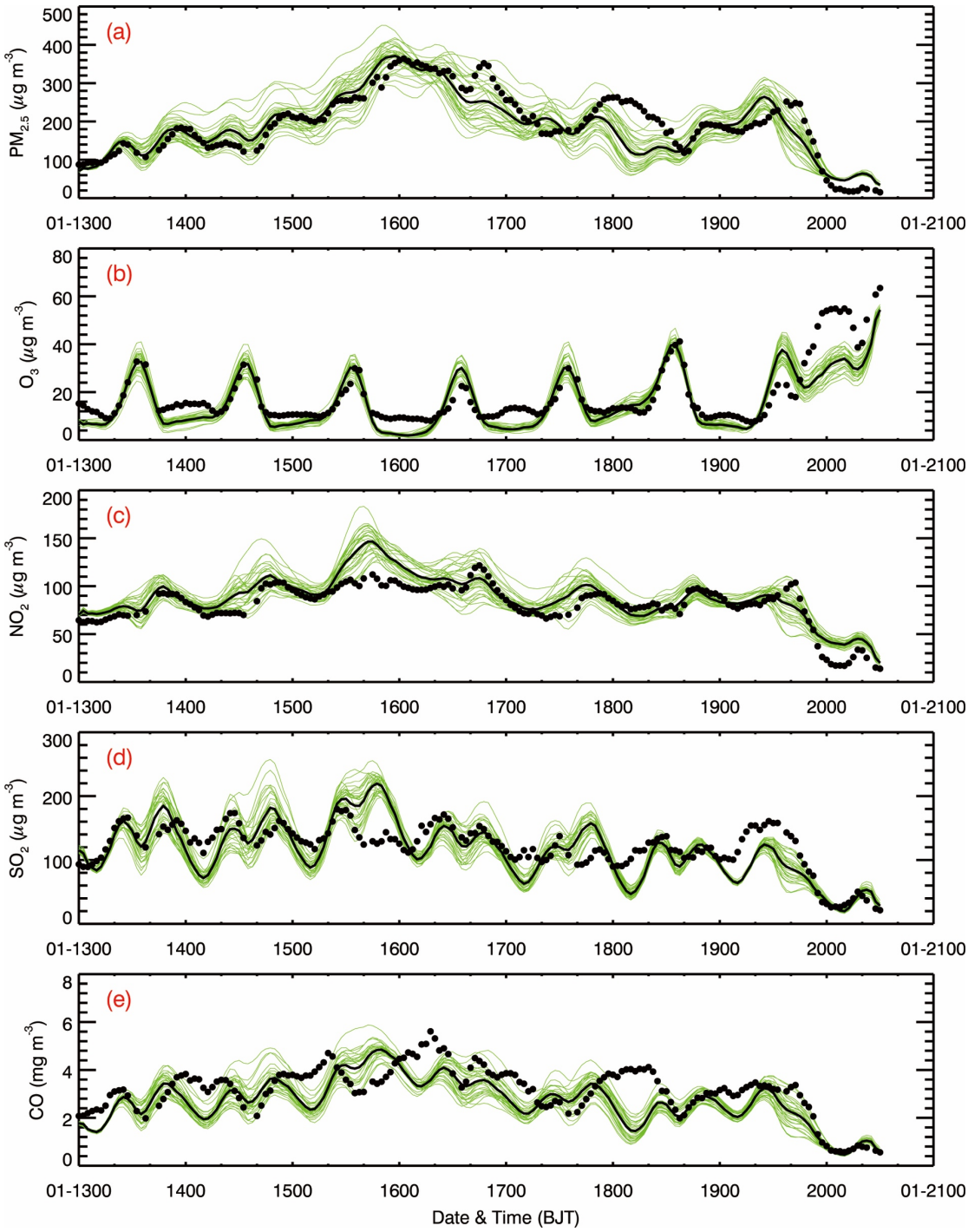

Figure 6 Temporal evolution of the (a) $PM_{2.5}$, (b) O_3, (c) NO_2, (d) SO_2, and (e) CO mass concentrations averaged over monitoring sites in BTH from each ensemble member (thin green lines), the ensemble mean (bold black line), and observations (black dots) from January 13 to 20, 2014.

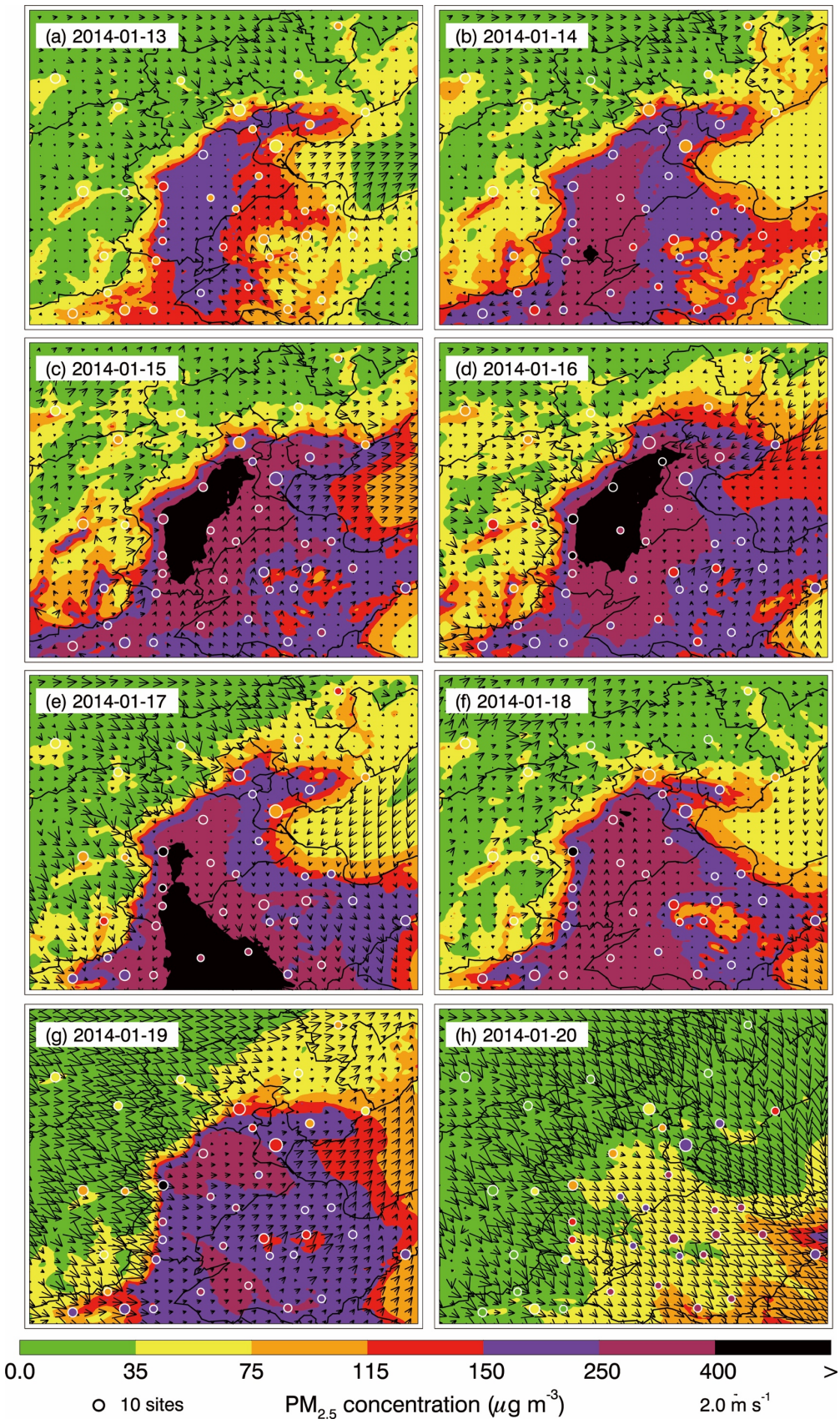

Figure 7 ENSM of the daily average surface $PM_{2.5}$ concentration distributions (colored contour) along with the ENSM of the daily average surface winds (black arrows) from January 13 to 20, 2014. The colored circles denote the $PM_{2.5}$ measurements in cities.

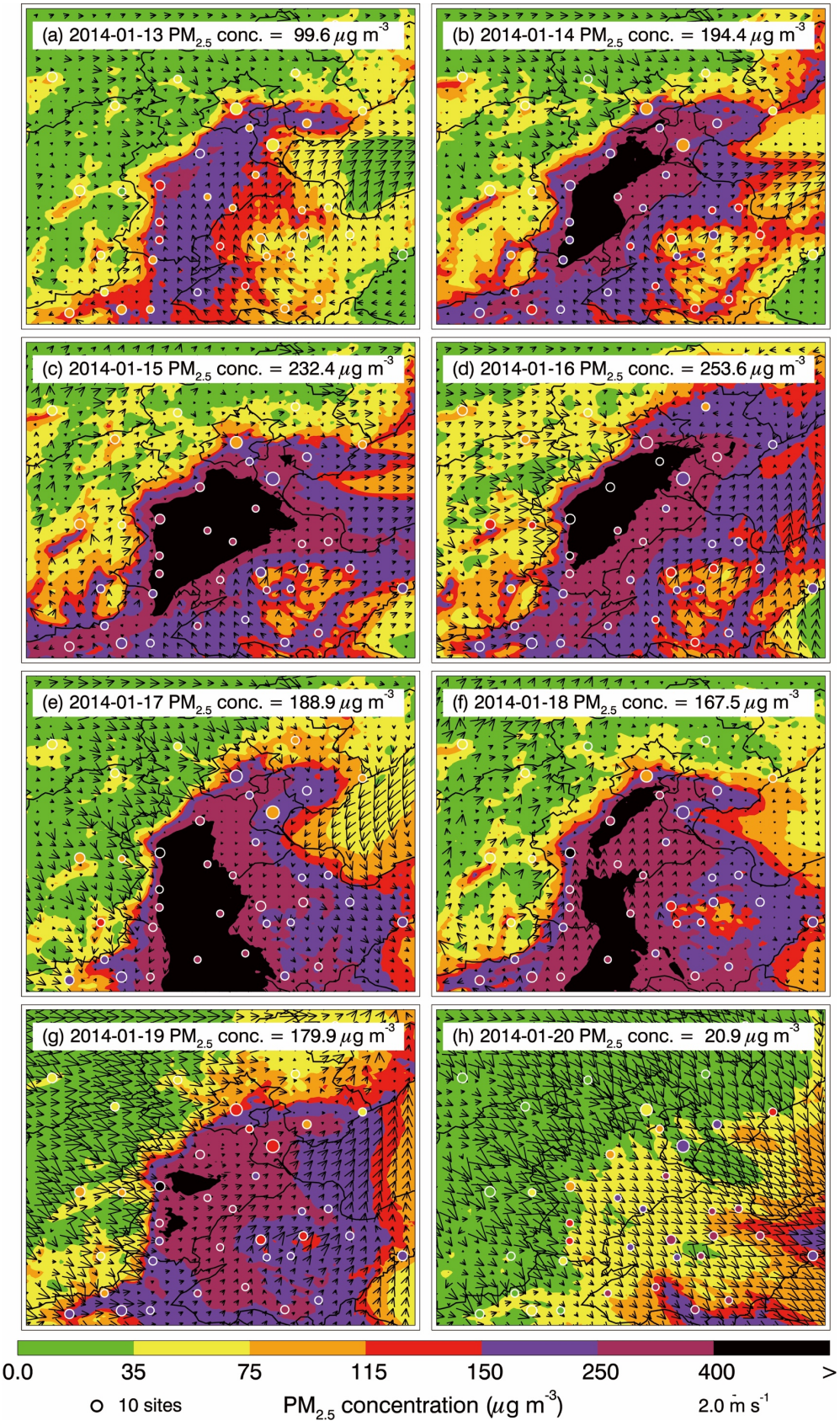

Figure 8 Same as Figure 7, but for the ensemble member of 16 with the highest simulated $PM_{2.5}$ concentration.

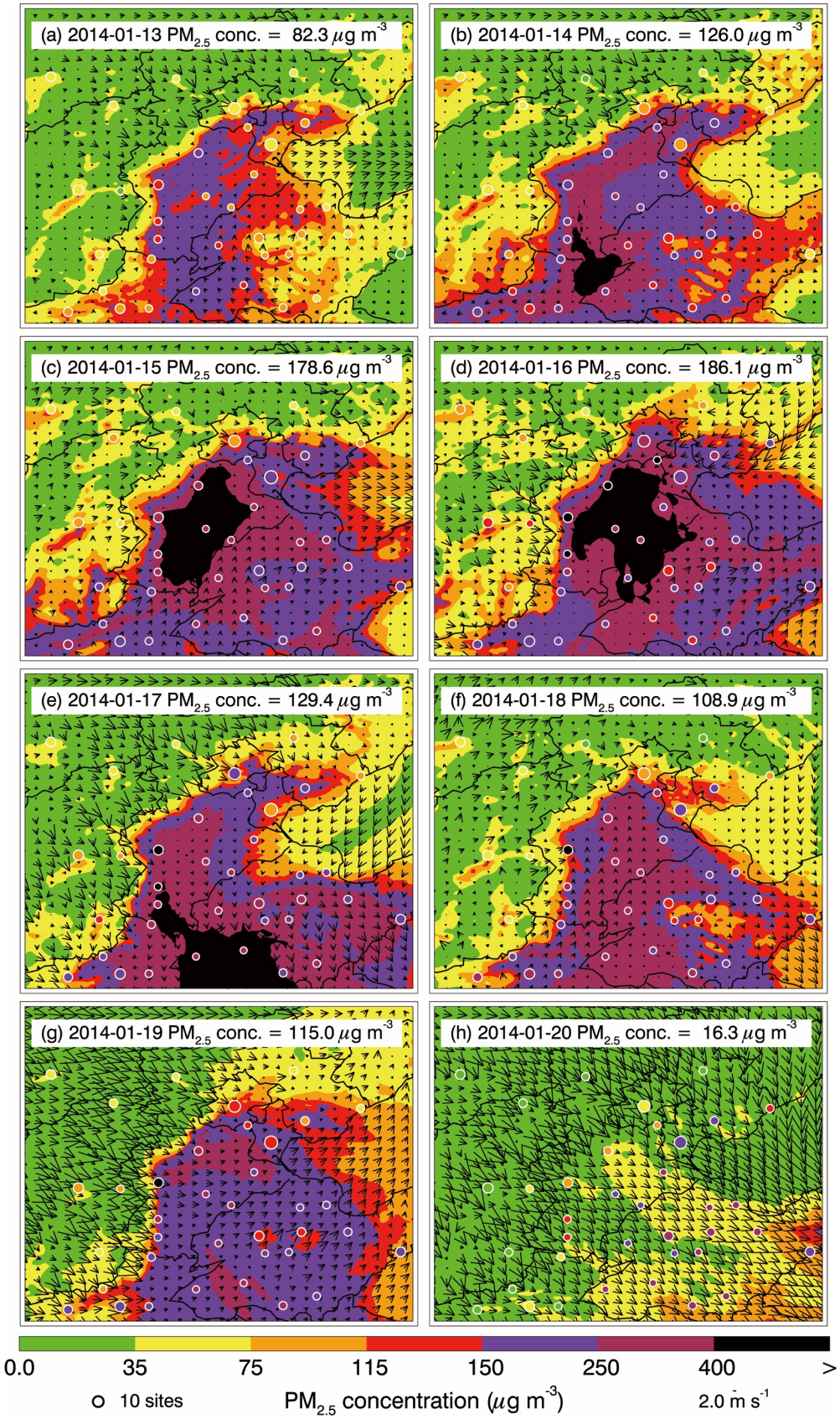

Figure 9 Same as Figure 7, but for the ensemble member of 30 with the lowest simulated $PM_{2.5}$ concentration.

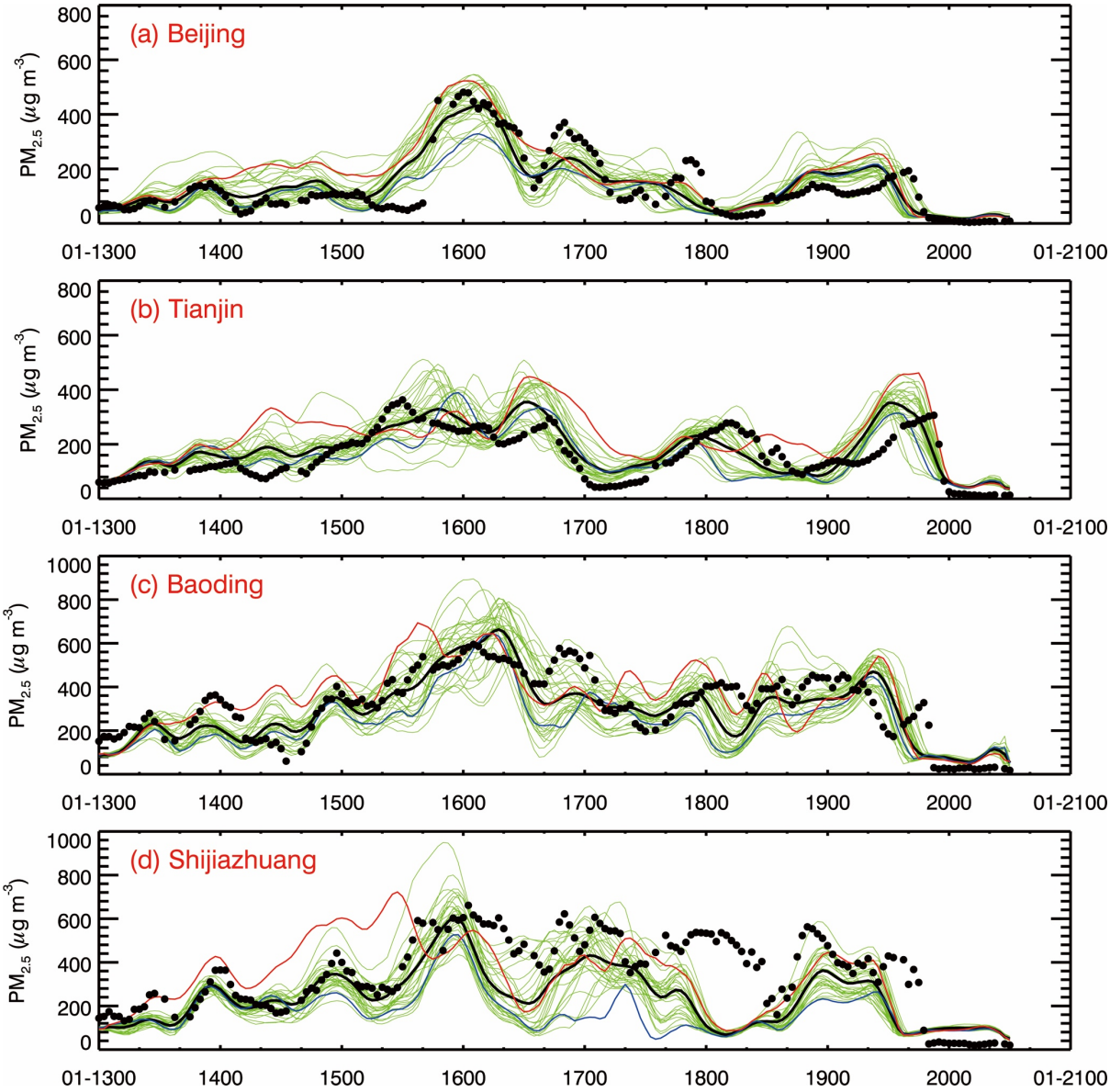

Figure 10 Temporal evolution of the $PM_{2.5}$ mass concentrations averaged in (a) Beijing, (b) Tianjin, (c) Baoding, and (d) Shijiazhuang from each ensemble member (thin green lines), the ensemble mean (bold black line), and observations (black dots) during the period from January 13 to 20, 2014. The red and blue lines represent the simulations in the members with highest and lowest $PM_{2.5}$ concentrations, respectively.